

Synthesis of Cs₃Cu₂I₅ Nanocrystals in a Continuous Flow System

Ksenija Arslanova, Patrick Ganswindt,* Tizian Lorenzen, Ekaterina Kostyurina, Konstantin Karaghiosoff, Bert Nickel, Knut Müller-Caspary, and Alexander S. Urban*

Achieving the goal of generating all of the world's energy via renewable sources and significantly reducing the energy usage will require the development of novel, abundant, nontoxic energy conversion materials. Here, a cost-efficient and scalable continuous flow synthesis of Cs₃Cu₂I₅ nanocrystals is developed as a basis for the rapid advancement of novel nanomaterials. Ideal precursor solutions are obtained through a novel batch synthesis, whose product served as a benchmark for the subsequent flow synthesis. Realizing this setup enabled a reproducible fabrication of Cs₃Cu₂I₅ nanocrystals. The effect of volumetric flow rate and temperature on the final product's morphology and optical properties are determined, obtaining 21% quantum yield with the optimal configuration. Consequently, the size and morphology of the nanocrystals can be tuned with far more precision and in a much broader range than previously achievable. The flow setup is readily applicable to other relevant nanomaterials. It should enable a rapid determination of a material's potential and subsequently optimize its desired properties for renewable energy generation or efficient optoelectronics.

1. Introduction

Ternary copper halide nanocrystals have been attracting growing attention as an alternative to lead-based halide perovskites for a broad range of optoelectronic applications.^[1,2] Their 0D crystal structure and self-trapped exciton mediated emission often lead to high photoluminescence quantum yields (PLQYs) in the deep UV region with outstanding stability at elevated temperatures and upon exposure to moisture. (The term "0D" crystal structure refers to the isolated nature on the molecular level of the copper iodide complexes – single copper iodide tetrahedra and edge-sharing dimers of tetrahedral and trigonal planar copper iodide complexes.)^[1,3-4] In contrast, iodide-based lead halide perovskites systems suffer from low ambient stability, the presence of toxic lead and can only cover emission

ranges at the low-energy end of the visible spectrum.^[5] To cover deep-UV emission with these systems, strongly quantum-confined particles or chloride-based compositions are required. These, in turn, necessitate more extensive effort to obtain high PLQYs in colloiddally stable systems for the former and suffer from intrinsic instability for the latter.^[6-8] Thus, ternary copper halide nanocrystal systems are a promising candidate to overcome these drawbacks. One such material, Cs₃Cu₂I₅, first studied over 30 years ago^[9] has exhibited an immense potential for a broad range of optoelectronic applications, such as deep-blue light-emitting diodes (LEDs), UV photodetectors or as fluorescent inks for encryption technologies in its nanocrystalline form.^[10-12] While several syntheses have been developed for these exciting nanocrystals, scalability and morphological control over the reaction products are still major obstacles for this material class.^[1,13,14] Reaction temperature has been determined to influence the nanocrystal geometry in hot-injection syntheses, with a transition from small spheres to larger anisotropic nanorods with increasing temperature.^[15] In the first implementation of a fully autonomous and self-optimizing continuous-flow-based synthesis, the CuI-precursor concentration and reaction temperature were determined to be the most influential parameters for the synthesis.^[16] While the 0D crystal structure of the material precludes quantum confinement effects due to nanocrystal size, a dependency of the PLQY on the size of the nanocrystals was previously observed and attributed to the number of surface

K. Arslanova, P. Ganswindt, A. S. Urban
Nanospectroscopy Group and Center for NanoScience
Faculty of Physics
Ludwig-Maximilians-Universität München
Königinstr. 10, 80539 München, Germany
E-mail: p.ganswindt@physik.lmu.de; urban@lmu.de

T. Lorenzen, K. Müller-Caspary
Department of Chemistry and Center for NanoScience
Ludwig-Maximilians-Universität München
Butenandtstr. 11, 81377 München, Germany

E. Kostyurina, B. Nickel
Soft Condensed Matter Group and Center for NanoScience
Faculty of Physics
Ludwig-Maximilians-Universität München
Geschwister-Scholl-Platz 1, 80539 München, Germany

K. Karaghiosoff
Department of Chemistry
Ludwig-Maximilians-Universität München
Butenandtstr.5-13, 81377 München, Germany

 The ORCID identification number(s) for the author(s) of this article can be found under <https://doi.org/10.1002/sml.202403572>

© 2024 The Author(s). Small published by Wiley-VCH GmbH. This is an open access article under the terms of the [Creative Commons Attribution-NonCommercial](https://creativecommons.org/licenses/by-nc/4.0/) License, which permits use, distribution and reproduction in any medium, provided the original work is properly cited and is not used for commercial purposes.

DOI: 10.1002/sml.202403572

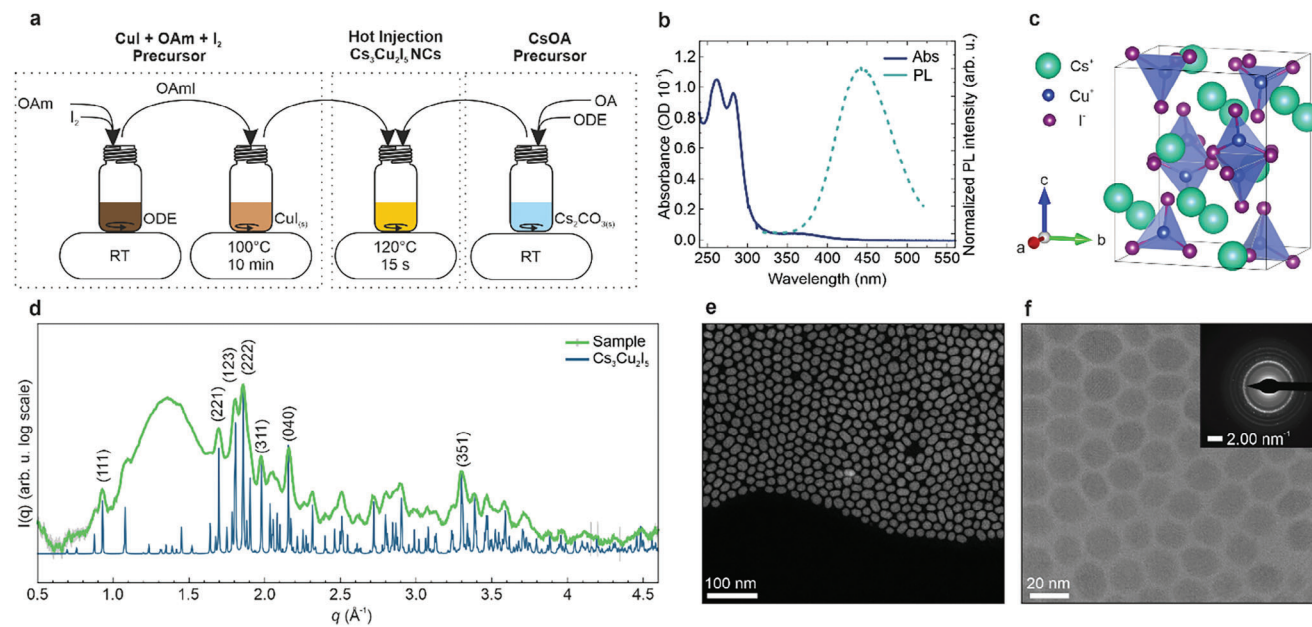


Figure 1. a) Schematic depiction of the hot-injection batch synthesis, showing the separate preparation of the copper precursor (left) and cesium precursor (right). b) Absorbance and normalized PL spectra of the obtained Cs₃Cu₂I₅ nanocrystal dispersion. The PL was normalized to the optical density (OD) of the sample at the excitation wavelength of 280 nm. c) Simplified depiction of the 0D crystal structure of Cs₃Cu₂I₅. d) Powder X-ray diffractogram showing sample diffraction in green and theoretical reference in blue.^[19] e) HR-STEM image and f) HR-TEM image of the nanocrystals with corresponding electron diffraction.

defects, highlighting the need for controlled surface coordination by ligands.^[14,17] Employing continuous flow systems for the fabrication of semiconductor nanocrystals has the dual advantage of having more precise control over reaction parameters and being able to screen reaction conditions significantly faster. Additionally, more moderate reaction conditions and lower precursor concentration due to increased heat- and mass transfer are possible, as well as a facile scale-up of the material production due to the continuous nature of the procedure.^[18] In the following, we present a facile and low-cost single-phase continuous flow approach for synthesizing Cs₃Cu₂I₅ nanocrystals. To obtain ideal precursors for this synthesis and to serve as a material baseline, we initially developed a novel hot-injection batch synthesis, which can be performed under ambient conditions. Based on this approach, we investigated different preparation methods for synthesizing Cs₃Cu₂I₅ nanocrystals under continuous flow conditions. After establishing a reliable and reproducible synthesis protocol, we systematically investigated the influence of the flow rate and the reaction temperature on the optical properties and morphology of the Cs₃Cu₂I₅ nanocrystals. The volumetric screenings reveal a direct dependence of the nanocrystal size on the flow rate and a transition in morphology from spherical particles to nanorods with increasing reaction temperature. Furthermore, we can optimize the nanocrystals' optical quality, as gauged by their PLQY, which reached the levels achieved through batch synthesis. This facile approach is readily applicable to other materials and should help to rapidly identify and optimize novel materials with higher potential for renewable energy generation and efficient energy usage.

2. Results and Discussion

As a prerequisite to establishing a continuous flow synthesis for Cs₃Cu₂I₅ nanocrystals, a batch synthesis was required to serve as a basis for designing the continuous flow reactor and to provide a reference to assess the viability of the flow integration. With only a limited number of viable batch syntheses in air reported, a novel batch, hot-injection approach for the synthesis of Cs₃Cu₂I₅ nanocrystals based on the direct use of copper(I) iodide in the presence of oleylamine (OAm) and iodine was developed.^[12–14,20] As outlined in **Figure 1**, the synthesis exploits an in situ formation of oleylammonium iodide (OAmI) as an external iodide source and dissolution agent for CuI as previously reported.^[21] The excess iodide concurrently serves as a reducing agent, suppressing the undesired formation of copper(II) salts and allowing the use of the precursor solution outside of a glove box.^[14] For the hot-injection synthesis, a cesium oleate precursor in 1-octadecene (ODE) and the copper precursor (CuI + OAm + I₂) were separately heated to 120 °C. The copper precursor was then rapidly injected into the cesium oleate solution, vigorously stirred for 15 s, and then immediately cooled to 0 °C with an ice-water bath. The reaction mixture was then purified before characterization (see Supporting Information for details). UV-vis spectroscopy reveals a strong absorption in the UV range, with two prominent peaks at 263 and 282 nm, the latter being attributed to excitonic absorption (Figure 1b). The photoluminescence (PL) spectra reveal a single, broad (full width at half maximum (FWHM) of 80 nm) emission peak centered at 440 nm, both indicative of self-trapped exciton emission.^[12,20] The sample

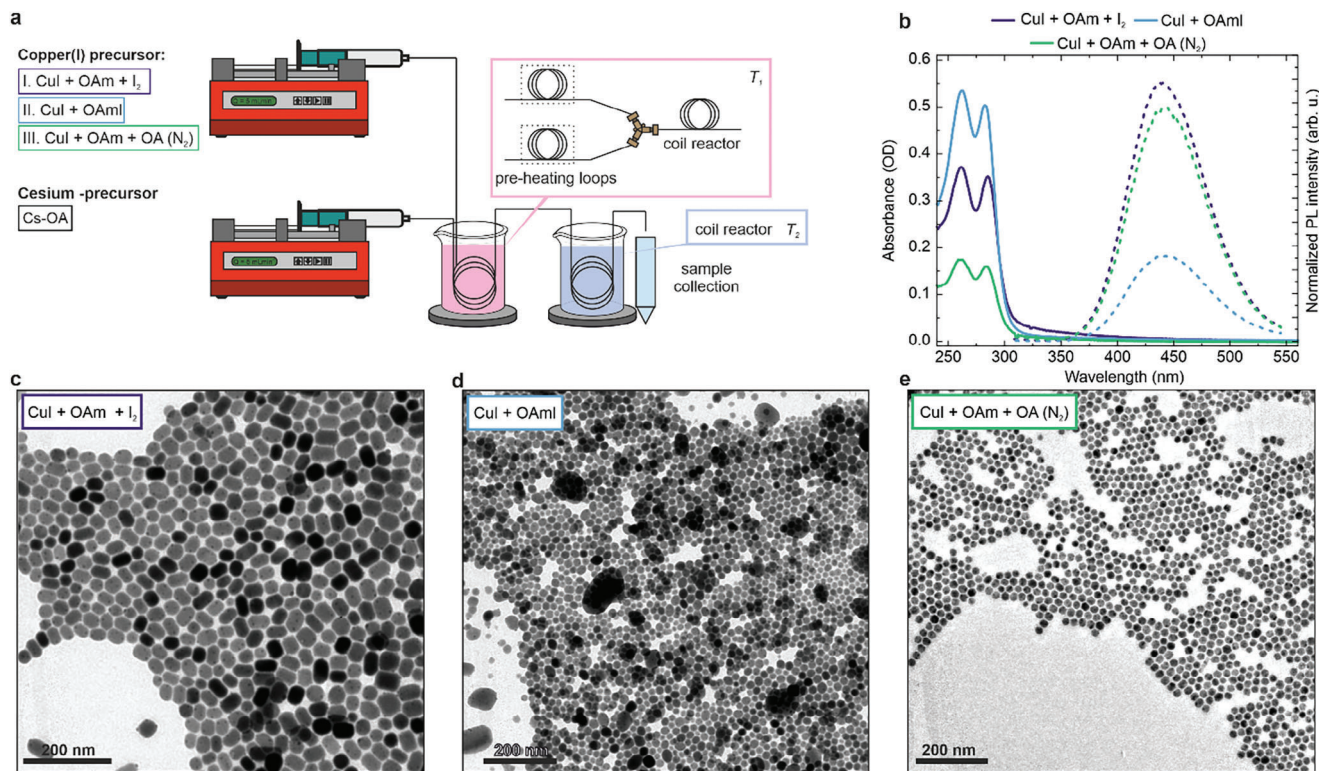


Figure 2. a) Schematic of the developed flow setup and the employed precursor solutions. b) Corresponding absorbance and relative PL of the samples prepared from the three different precursors. c–e) BF-TEM images of the respective nanoparticles were obtained from the different precursor approaches.

possesses a robust PLQY of 21.7%, a respectable value in light of the reported size dependence of the PLQY for this material, which is attributed to an increase of surface defect states at smaller sizes as well as the introduction of non-emitting trap states by the organic ligand shell.^[14,17] Powder X-ray diffraction (PXRD) confirmed the material to be $\text{Cs}_3\text{Cu}_2\text{I}_5$, which crystallizes in the space group Pnma (No.62) (Figure 1c,d). No undesired secondary phases, such as CsI or CuI , were detected, a testament to the purity and high quality of the sample (see Figure S1, Supporting Information).^[22–24] High-resolution scanning transmission electron microscopy (HR-STEM) shows the material to comprise regular, round, and partially elongated nanocrystals with an average diameter of 17.3 nm (Figure 1e). The electron diffraction pattern obtained from high-resolution transmission electron microscopy (HR-TEM) revealed some of the material's lattice planes, which correlated with theoretical values, further confirming the crystal structure (Figure 1f; Table S1, Supporting Information).^[22] The nanocrystals displayed excellent stability, with the optical properties and morphology preserved after storage under ambient conditions for six months (see Figure S2, Supporting Information).

Based on the developed hot-injection batch approach, we designed a continuous flow system composed of two precursor syringes, separate pre-heating loops, a Y-inlet for precursor mixing combined with a heated coil reactor (T_1), and a cooling section (T_2) with subsequent sample collection as shown in Figure 2a (for a more detailed description of the continuous flow integration see section Sections S1 and S2, Supporting Information). We adopted a single-phase flow approach to minimize system com-

plexity by achieving precursor mixing at the Y-inlet and in the coiled reactor.^[25]

To avoid precipitation inside the syringes or clogging of the flow system, we modified the precursor solutions from those used in the batch synthesis.^[26] To facilitate stability at room temperature, we adjusted the concentration of both precursor solutions to 0.01 M and increased the OA content in the cesium-precursor (to a Cs:OA ratio of 1:13).^[13] The resulting material was collected and purified before further characterization (see Section S2, Supporting Information). As shown in Figure 2b, the resulting product exhibited the same qualitative optical properties as the material obtained from the batch synthesis. The optical density at the excitation wavelength of 280 nm of the continuous flow sample after identical purification is an order of magnitude higher than the batch sample, indicating an improved reaction yield. The sample emits strong PL, confirmed by a PLQY of over 27.8%, signifying both excellent quality and purity of the in-flow prepared nanocrystals. TEM micrographs show regular nanocrystals with an elongated shape, similar to the batch synthesis (Figure 2c), with an average size of 24 nm, roughly an order of magnitude smaller than previously achieved with other continuous flow systems.^[16] Dynamic light scattering measurements confirm the monodisperse nature of the sample with only a single particle species present (see Figure S3, Supporting Information). Despite these impressive results, the procedure suffered from reproducibility issues, likely caused by the copper-precursor solution (for a detailed explanation, see Section S2, Supporting Information). Accordingly, despite this being the first time that colloiddally stable $\text{Cs}_3\text{Cu}_2\text{I}_5$ nanocrystals

could be successfully synthesized from a single-phase continuous flow setup, we excluded the use of this precursor solution for further investigation of the system.

As determined previously, OAmI is responsible for the dissolution and stabilization of CuI in the precursor solution and the nanocrystals obtained after the synthesis.^[21] Consequently, to circumvent the issues encountered with the first precursor, OAmI was synthesized according to a modified approach from Maceiczky et al. and directly employed in a stoichiometric ratio of 2:3 between CuI and OAmI as the second precursor to be assessed for the continuous flow synthesis (Figure 2a; Section S2 and Table S2, Supporting Information).^[27] The ratio was crucial to overcome the low solubility of CuI in 1-octadecene. The synthesis also yielded regular nanocrystals (Figure 2d) with the characteristic optical properties (light blue graphs in Figure 2b), confirming the desired Cs₃Cu₂I₅ composition. However, the sample displayed low PLQY values of only 2.8% alongside the significant presence of impurities observed in TEM micrographs (Figure 2d) and low colloidal stability as it precipitated after 24 h (Figure S6a, Supporting Information). We attribute the impurities and the low optical quality to the excess of OAmI employed in the synthesis. Based on the TEM micrographs, the ligand appears to aggregate, leading to insufficient passivation and stabilization of the obtained nanocrystals, which results in low colloidal stability and diminished PLQYs. Furthermore, PXRD of the sample does not indicate the presence of any major amounts of undesired secondary phases, such as oxide formation on the nanocrystals' surface, which could have deteriorated the PLQY and reduced colloidal stability (Figure S7, Supporting Information). In addition, photoluminescence excitation (PLE) spectra of the sample also show no hint of additional optically active species, which could impact the PLQY of the sample (Figure S6b, Supporting Information). While the presence of minor amounts of surface oxide phases cannot be entirely excluded from the PXRD, we attribute the lack of stability and low sample quality mainly to the aggregation of OAmI. Therefore, this precursor was also excluded from further investigation.

The quality and reproducibility issues of the first two precursors likely stemmed from using an external iodide source or the excess ligand necessary. Thus, we prepared the copper and cesium precursors separately under inert conditions with a Schlenk line.^[16] Without an external iodide source, and in the absence of ambient oxygen, the copper(I) precursor could directly be prepared at the required dilute concentrations and remained stable at room temperature (see Section S2, Supporting Information). Using this precursor, the resulting nanocrystals are highly homogeneous (Figure 2e), with an average size of 23.4 nm. The optical properties align with the previous syntheses (turquoise graphs in Figure 2b), with a low optical density at 280 nm likely due to the smaller size of the nanocrystals and possibly lower reaction yields. However, the high relative PL intensity and a PLQY of 18.7% indicate excellent material quality. Most importantly, the resulting nanocrystals were extremely stable, and the method was highly reproducible, yielding nearly identical results between different syntheses. Further characterization confirmed the high quality and purity of the sample: HR-STEM and electron diffraction confirmed the crystallinity of the nanoparticles and the theoretical lattice spacings of the desired 0D Cs₃Cu₂I₅ phase (see Figure S8, Supporting Informa-

tion). Energy-dispersive X-ray spectroscopy (EDX) mapping of the particles revealed a homogeneous distribution of all elements (Figure S9, Supporting Information), and PXRD analysis did not detect any significant amount of impurities (Figure S10, Supporting Information). These results confirm that operating in a stoichiometric excess of copper has a positive influence on the quality of the nanocrystals.^[15,16]

Having established a successful and reliable continuous flow synthesis, we turned to optimizing the resulting Cs₃Cu₂I₅ nanocrystals. The most critical parameters are the reactor temperature and the overall flow rate, which controls the total residence time. This is inversely proportional to the volumetric flow rate, Q , in mL min⁻¹ and is given by $t_{\text{synth}} = C/Q$, with a constant $C = 48.6$ s mL min⁻¹ (employed flow rates and residence times are listed in Table S5, Supporting Information). To understand how the nanocrystals grow, we varied the flow rate from 1.25 to 10 mL min⁻¹, corresponding to residence times of 40–5 s at a reaction temperature of 75 °C (Figure 3a–d). At 10 mL min⁻¹ ($t_{\text{synth}} = 5$ s), the resulting nanocrystals are slightly irregularly shaped, exhibiting a homogeneous size of only 17 nm, significantly smaller than the nanocrystals obtained in the batch synthesis. The UV–vis spectrum displays the expected two peaks, with nearly no absorbance at higher wavelengths; however, the absorbance overall is relatively low.

The PL was detectable with a PLQY of 12.3%. Increasing the synthesis time to 10 s (5 mL min⁻¹) leads to far more regular, hexagonal to nearly spherical nanocrystals with an increased size of 24 nm. The absorbance increases nearly fourfold with only a small shoulder on the long wavelength side. The dispersions are also significantly brighter and exhibit a PLQY of 18.3%. A further increase of the residence time to 20 s (2.5 mL min⁻¹) leads to a significant increase of the nanocrystal size to 40 nm, with a pronounced size dispersion and a shape change toward a cubic shape. The absorbance is nearly identical in the UV range compared to the previous sample; however, the absorbance increases notably for $\lambda > 300$ nm. These nanocrystals also exhibit a further increase in PLQY up to 20.6%, on par with the batch synthesis value. At the longest synthesis time (40 s), the nanocrystals grow further; however, it becomes difficult to determine the exact size as they appear to aggregate. This coincides with a significantly diminished absorbance in the UV (while the long wavelength shoulder remains large) and a diminished PL intensity with a PLQY of only 9.8%.

Overall, the flow rate screening reveals an increase in nanocrystal size and a transition from predominantly spherical and hexagonal to rectangular and cubic morphology with increasing synthesis time (decreasing flow rate). Additionally, absorbance and PLQY increase initially before declining at the lowest flow rate. As the average nanocrystal size increases only by ca. 7 nm between 5 and 10 s residence time (10 and 5 mL min⁻¹), yet the absorbance increases by a factor of 4, nucleation appears to be dominating the reaction during the first 10 s. This matches a previous study that found slow initial growth periods for Cs₃Cu₂I₅ nanorods from batch syntheses.^[15] After 20 s residence time (2.5 mL min⁻¹), the average diameter increases by 16 nm while the absorbance remains identical, showing that growth dominates after the first 10 s of nucleation. Extending the residence time to 40 s (1.25 mL min⁻¹), growth stagnates at longer reaction times while colloidal stability and sample quality concurrently

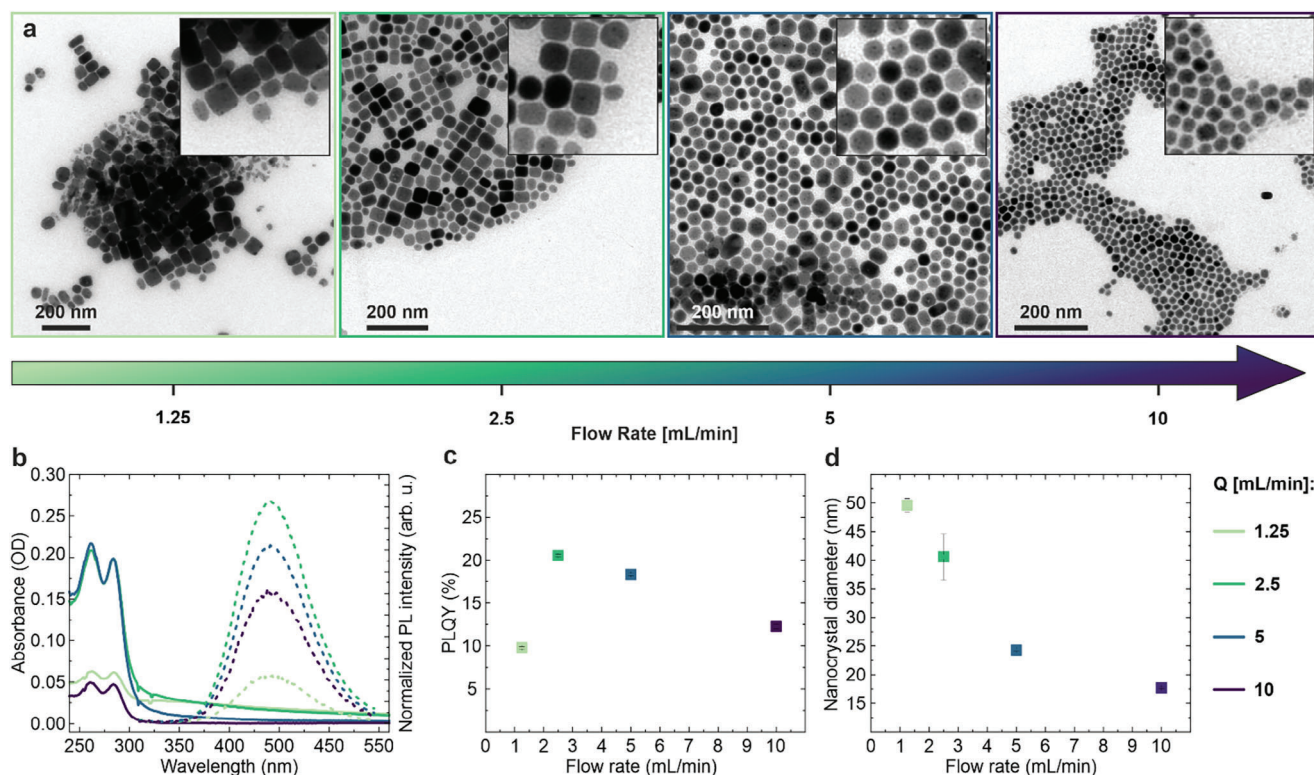


Figure 3. a) TEM micrographs of samples prepared at different flow rates with a reaction temperature of 75 °C. b) Absorbance and normalized PL intensity of the corresponding dispersions. c) PLQY of all samples investigated in the flow rate screening. d) Average size of the obtained nanocrystal diameters as determined from the TEM micrographs.

deteriorate substantially. The results of this measurement series can be used to target specific nanocrystal sizes while keeping the optical properties nearly constant by simply adjusting the flow rate.

With the ideal flow rate determined, we turned to the second crucial parameter, the temperature. Setting the flow rate to 5 mL min⁻¹, we varied the synthesis temperature between 40 and 140 °C. At 40 °C, the nanocrystals display morphologies ranging from spheres and cubes to elongated hexagons, with an average diameter (44 nm) almost twice as large as the nanocrystals obtained at 75 °C in the flow rate screening (Figure 4d; Figure S14, Supporting Information). While the high absorbance indicates a moderate reaction yield, the weak relative PL intensity and PLQY of 12.3% of the sample indicate poor material quality (Figure 4b,c). As the reactor temperature increases, the morphology slowly changes from hexagonal to more cubic nanocrystals, with the average size decreasing significantly up to 80 °C. At 100 °C, the nanocrystals form as predominantly very regular nanorods, with an average size of 23 × 44 nm. At the two highest temperatures employed, the final dispersion turned turbid, indicating severe material aggregation (Figures S12 and S13, Supporting Information). This also prevented us from acquiring TEM micrographs of the resulting material. The absorption in the UV range increases slightly up to 60 °C and then drops continuously, while the PLQY reaches a maximum of 20.5% at 80 °C before dropping off and reaching 5% at 140 °C.

The temperature screening for the continuous flow synthesis of Cs₃Cu₂I₅ nanocrystals indicates that aggregate formation or

uncontrolled nanocrystal growth occurs for either too-low or too-high reaction temperatures. At low temperatures, nucleation appears inhibited, causing the growth of few but large nanocrystals of poor quality. At too high temperatures, an anisotropic growth of the nanocrystals with low yields seems to transpire, suggesting a fast growth rate that competes with the nanocrystal nucleation, causing defect-rich nanocrystals to form and limiting the reaction yield. Furthermore, the reaction series demonstrated a clear morphological transition from polydisperse and irregular shapes at low temperatures to more regular, anisotropic morphologies at higher temperatures. Additionally, these experiments revealed a temperature dependence of nucleation and growth rate, with the latter being favored at higher temperatures and the former peaking at an intermediate temperature range around 60 °C.

In summary, we have developed a facile and low-cost single-phase continuous flow synthesis for Cs₃Cu₂I₅ nanocrystals. As a basis for the flow synthesis, a novel batch procedure was developed that allows the preparation of the material under ambient conditions and with the direct use of CuI as a precursor. The procedure yields highly monodisperse nanocrystals of high optical quality and outstanding stability. Subsequently, a low-cost continuous flow system was developed, and three different copper precursors were assessed, yielding a reliable synthesis of high-quality and homogenous nanocrystals that can be prepared at lower temperatures and with higher PLQYs compared to most batch syntheses and other continuous flow approaches. To gain further insights into the formation of the

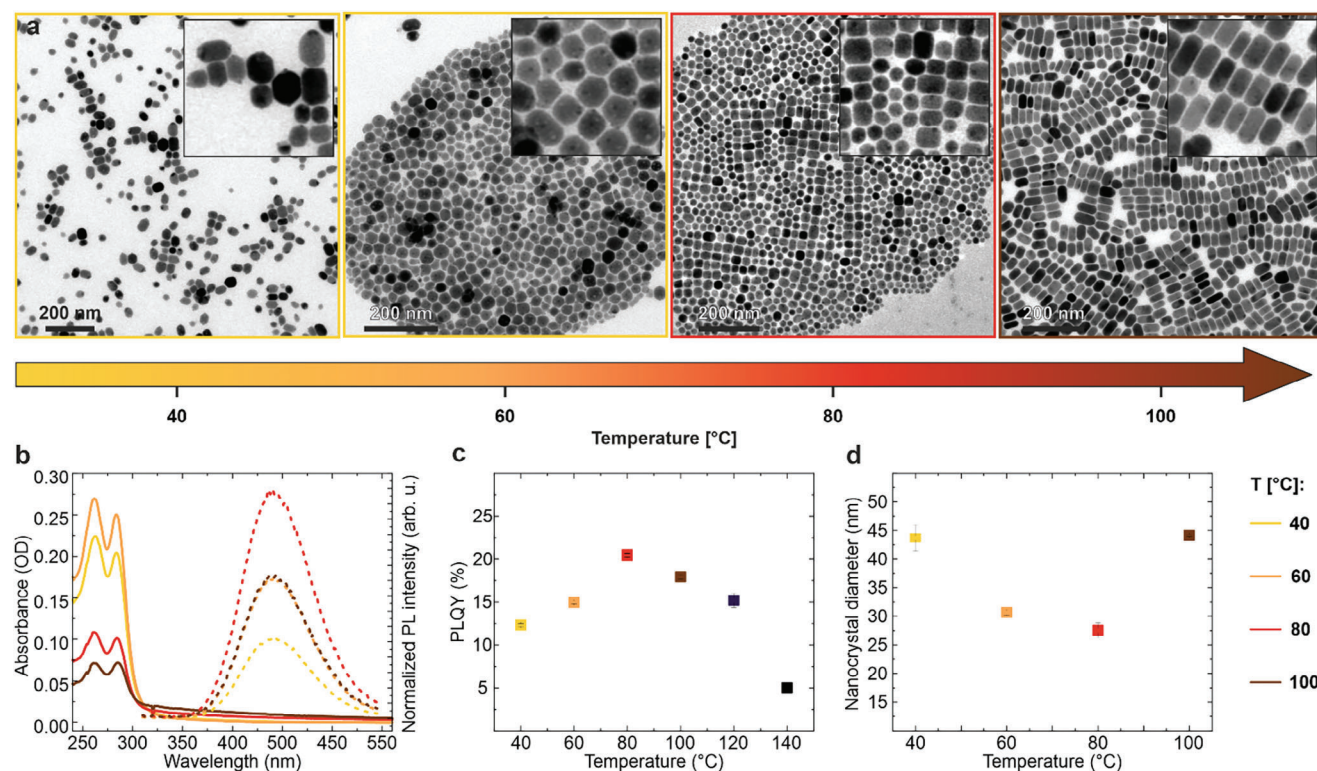


Figure 4. a) TEM micrographs of samples prepared at different T_1 reactor temperatures with a flow rate of 5 mL min^{-1} . b) Absorbance and normalized PL intensity of the corresponding dispersions. c) PLQY of all samples investigated during temperature screening. d) Average size of the obtained nanocrystal diameters as determined from the TEM micrographs.

nanocrystals, a screening of the flow rate and reaction temperature was conducted, revealing a strong dependence of the nanocrystals' size on the flow rate and a change of the morphology from regular spherical nanocrystals to nanorods for increasing reaction temperatures. Furthermore, the screening revealed an optimum for the PLQY, approaching 21% for nanocrystal sizes below 20 nm. The work highlights the beneficial influence continuous flow manufacturing can have on the quality of semiconductor nanocrystals. Through more precise control over reaction conditions, increased heat and mass transfer, and access to shorter reaction times with better overall reproducibility compared to batch syntheses, continuous flow syntheses present a powerful tool for obtaining and investigating high-quality semiconductor nanocrystals, which is crucial for advancing and developing highly efficient energy conversion materials for optoelectronic applications.

3. Experimental Section

Chemicals: All reagents were used as received without further purification: copper(I) iodide (CuI, for synthesis, Sigma–Aldrich), caesium carbonate (Cs_2CO_3 , 99%, Sigma–Aldrich), 1-octadecene (ODE, 90%, Sigma–Aldrich), oleylamine (OAm, 70%, Sigma–Aldrich), oleic acid (OA, 90%, Sigma–Aldrich), iodine (I_2 , sublimed, VWR), hydroiodic acid (HI, 57%, Sigma–Aldrich), magnesium sulfate (MgSO_4 , VWR), sodium chloride (NaCl, VWR), acetone (99.9%, Sigma–Aldrich), n-Hexane (97%, Sigma–Aldrich), ethyl acetate (EtOAc, VWR).

Hot Injection Batch Synthesis of $\text{Cs}_3\text{Cu}_2\text{I}_5$ Nanocrystals—Preparation of 0.1 M CsOA precursor: Cs_2CO_3 (163 mg, 0.5 mmol) was mixed with OA (4.1 mL, 13 mmol) and 5.9 mL ODE in a glass vial. Then, the vial was heated on a hot plate at 120 °C until the caesium salt was completely dissolved. The precursor was cooled down to room temperature and stored under ambient conditions.

Hot Injection Batch Synthesis of $\text{Cs}_3\text{Cu}_2\text{I}_5$ Nanocrystals—Preparation of 0.4 M OAm/ I_2 Additive: Iodine (252 mg, 1 mmol) was mixed with OAm (1.66 mL, 5 mmol) and 3.33 mL ODE in a glass vial. The mixture was stirred for approx. 30 min.

Hot Injection Batch Synthesis of $\text{Cs}_3\text{Cu}_2\text{I}_5$ Nanocrystals—Preparation of 0.1 M CuI + OAm + I_2 Precursor: To prepare a 0.1 M precursor solution, CuI (190 mg, 1 mmol) was mixed with an OAm/ I_2 additive (0.4 M, 2 mL) and 8 mL of ODE in a glass vial. Then, the vial was heated on a hot plate at 120 °C until the copper salt was completely dissolved. The precursor was cooled down to room temperature and stored under ambient conditions.

Hot Injection Batch Synthesis of $\text{Cs}_3\text{Cu}_2\text{I}_5$ Nanocrystals—Hot Injection Batch Synthesis: 1.5 mL of 0.1 M CsOA precursor was mixed with 5 mL ODE and heated to 120 °C. 0.1 M “CuI + OAm + I_2 ” precursor was heated to 120 °C and then 1 mL of the “CuI + OAm + I_2 ” precursor was rapidly injected into the CsOA/ODE mixture. The reaction mixture was stirred for 15 s before it was cooled down to 0 °C by placing the vial into a water-ice bath. The frozen reaction mixture was then allowed to warm to room temperature, transferred to a Falcon tube, and centrifuged at 5000 rpm for 5 min. The resulting sediment was isolated and resuspended in 2 mL of hexane.

Continuous-Flow Procedure—Preparation of 0.01 M CsOA Precursor: Cs_2CO_3 (163 mg, 0.5 mmol) was mixed with OA (4.1 mL, 13 mmol) and 5.9 mL ODE in a glass vial. Then, the vial was heated on a hot plate at 120 °C until the caesium salt was completely dissolved. The precursor was cooled down to room temperature and stored under ambient conditions. Before the synthesis, the 0.1 M precursor

solution was diluted with ODE 1:9 to obtain a 0.01 M precursor solution.

Continuous-Flow Procedure—Preparation of 0.4 M OAm I₂ Additive: Iodine (252 mg, 1 mmol) was mixed with OAm (1.66 mL, 5 mmol) and 3.33 mL ODE in a glass vial. The mixture was stirred for ≈30 min.

Continuous-Flow Procedure—Preparation of 0.01 M CuI + OAm + I₂ Precursor: CuI (57 mg, 0.3 mmol) was mixed with an OAm/I₂ additive (0.4 M, 1.125 mL) and 1.875 mL of ODE in a glass vial. Then, the vial was heated on a hot plate at 120 °C until the copper salt was completely dissolved. Before the synthesis, the 0.1 M precursor solution was diluted with ODE 1:9 to obtain a 0.01 M precursor solution.

Continuous-Flow Procedure—Preparation of 0.5 M OAmI Additive: Oleylammonium iodide was synthesized according to the synthesis of Maceiczky et al.^[27] Oleylamine (12.5 mL, 38 mmol) was dissolved in absolute ethanol (100 mL). The mixture was cooled to 0 °C, and hydroiodic acid (57%, 10 mL, 76 mmol) was added dropwise. The mixture was left to stir overnight at room temperature. Subsequently, the ethanol was removed using a rotary evaporator, and the aqueous phase was extracted with ethyl acetate (3 × 100 mL). The organic phase was washed with brine (3 × 50 mL) and dried over MgSO₄. Afterward, the solvent was removed under vacuum. The resulting product was used without further purification. To obtain 0.5 M OAmI solution in ODE, OAmI (988.5 mg, 2.5 mmol) was dissolved at 100 °C in 5 mL ODE.

Continuous-Flow Procedure—Preparation of 0.01 M CuI + OAmI Precursor: CuI (38 mg, 0.2 mmol) was mixed with OAmI additive (0.5 M, 0.6 mL), OAm (1 mL, 3 mmol), and 1.4 mL ODE in a glass vial. Then, the vial was heated on a hot plate at 120 °C until the copper salt was completely dissolved. Before the synthesis, the 0.1 M precursor solution was diluted with ODE 1:9 to obtain a 0.01 M precursor solution.

Continuous-Flow Procedure—Preparation of 0.01 M CsOA Precursor (N₂): Cs₂CO₃ (32 mg, 0.1 mmol) was mixed with OA (0.82 mL, 2.6 mmol) and 19.18 mL ODE in a three-necked round bottom flask. The flask was heated to 120 °C for 1 h under vacuum and cooled down to RT, resulting in a 0.01 M CsOA precursor solution.

Continuous-Flow Procedure—Preparation of 0.01 M CuI + OA + OAm Precursor (N₂): CuI (38 mg, 0.2 mmol) was mixed with 10 mL ODE in a three-necked round bottom flask. The flask was heated to 120 °C under vacuum for 30 min to degas the mixture. Simultaneously, oleic acid (1 mL, 3 mmol) and oleylamine (1 mL, 3 mmol) ligands were mixed with 8 mL ODE in a separate three-necked round bottom flask and degassed at 120 °C under vacuum for 30 min. After that, 10 mL of OA/OAm/ODE mixture was transferred to the CuI/ODE mixture via a syringe. The resulting precursor solution was heated for a further 30 min at 120 °C and then cooled down to RT. The 0.01 M CuI + OA + OAm (N₂) precursor was obtained as a clear solution.

Absorbance and PL Spectroscopy: PL spectra and UV–vis absorbance spectra of purified Cs₃Cu₂I₅ nanocrystal dispersions were measured with a commercial FluoroMax-4Plus spectrometer equipped with a xenon arc lamp and an F-3031 transmission accessory (HORIBA Scientific). The excitation wavelength for PL spectra was set to 280 nm. For PLQY measurements a Quanta-phi integrating sphere was employed and the samples were excited at 300 nm.

Dynamic Light Scattering: Dynamic light scattering (DLS) measurements were performed on a Malvern Zetasizer Pro.

Electron Microscopy: High-resolution STEM and TEM imaging was performed using a probe-corrected FEI Titan Themis operated at an acceleration voltage 300 kV. STEM images were recorded at a semi-convergence angle of 16.6 mrad at a camera length of 196 mm using a Fischione HAADF detector. A Super-X detector was used for EDS imaging. Specimen preparation was carried out by drop casting onto TEM grids (Quantifoil R2/2, 2 nm ultrathin carbon).

Powder X-Ray Diffraction: Powder X-ray diffraction data was collected at the laboratory X-ray scattering setup at the soft condensed matter chair of LMU Munich. The setup uses molybdenum K α radiation (0.71 Å) of a microfocus X-ray source (Xenos) collimated to a beam size of ≈1 × 1 mm. Dispersions of NCs in n-hexane were drop-casted onto adhesive tape (3 M Scotch Magic 810) and measured in transmission

mode after drying. The data was collected using a Dectris Pilatus 100K detector.

Supporting Information

Supporting Information is available from the Wiley Online Library or from the author.

Acknowledgements

This project was funded by the European Research Council Horizon 2020 through the ERC Grant Agreement PINNACLE (759744); by the Deutsche Forschungsgemeinschaft (DFG under Germany's Excellence Strategy EXC 2089/1-390776260 and by the Bavarian State Ministry of Science, Research and Arts through the grant "Solar Technologies go Hybrid (SolTech)".

Open access funding enabled and organized by Projekt DEAL.

Conflict of Interest

The authors declare no conflict of interest.

Author Contributions

K.A. and P.G. contributed equally to this work. The manuscript was written through the contributions of all authors. All authors have given approval to the final version of the manuscript.

Data Availability Statement

The data that support the findings of this study are available from the corresponding author upon reasonable request.

Keywords

continuous flow synthesis, flow chemistry, morphology control, semiconductor nanocrystals, synthesis optimization, ternary copper halides

Received: May 3, 2024
Revised: June 19, 2024
Published online: July 14, 2024

- [1] Y. Li, Z. Zhou, N. Tewari, M. Ng, P. Geng, D. Chen, P. K. Ko, M. Qammar, L. Guo, J. E. Halpert, *Mater. Chem. Front.* **2021**, *5*, 4796.
- [2] T. Jun, K. Sim, S. Iimura, M. Sasase, H. Kamioka, J. Kim, H. Hosono, *Adv. Mater.* **2018**, *30*, 1804547.
- [3] Z. Guo, J. Li, R. Pan, J. Cheng, R. Chen, T. He, *Nanoscale* **2020**, *12*, 15560.
- [4] Z. Ma, Z. Shi, C. Qin, M. Cui, D. Yang, X. Wang, L. Wang, X. Ji, X. Chen, J. Sun, D. i Wu, Y. u Zhang, X. J. Li, L. Zhang, C. Shan, *ACS Nano* **2020**, *14*, 4475.
- [5] K. Antami, F. Bateni, M. Ramezani, C. E. Hauke, F. N. Castellano, M. Abolhasani, *Adv. Funct. Mater.* **2022**, *32*, 2108687.
- [6] S. Martin, N. A. Henke, C. Lampe, M. Döblinger, K. Frank, P. Ganswindt, B. Nickel, A. S. Urban, *Adv. Opt. Mater.* **2024**, *12*, 2301009.
- [7] Y. Hong, C. Yu, H. Je, J. Y. Park, T. Kim, H. Baik, G. M. Tomboc, Y. Kim, J. M. Ha, J. Joo, C. W. Kim, H. Y. Woo, S. Park, D. H. Choi, K. Lee, *Adv. Sci.* **2023**, *10*, 2302906.

- [8] S. Samiei, E. Soheyli, K. Vighnesh, G. Nabiyouni, A. L. Rogach, *Small* **2024**, *20*, 2307972.
- [9] K. P. Bigalke, A. Hans, H. Hartl, *Z. für Anorg. Allg. Chem.* **1988**, *563*, 96.
- [10] L. Wang, Z. Shi, Z. Ma, D. Yang, F. Zhang, X. Ji, M. Wang, X. u Chen, G. Na, S. Chen, D. i Wu, Y. u Zhang, X. Li, L. Zhang, C. Shan, *Nano Lett.* **2020**, *20*, 3568.
- [11] X. Zhao, Y. Tao, J. Dong, Y. Fang, X. Song, Z. Yan, *ACS Appl. Mater. Interfaces* **2022**, *14*, 43490.
- [12] F. Gao, X. Zhu, Q. Feng, W. Zhong, W. Liu, H. Xu, Y. Liu, *Nano Energy* **2022**, *98*, 107270.
- [13] Y. Li, P. Vashishtha, Z. Zhou, Z. Li, S. B. Shivarudraiah, C. Ma, J. Liu, K. S. Wong, H. Su, J. E. Halpert, *Chem. Mater.* **2020**, *32*, 5515.
- [14] Z. Luo, Q. Li, L. Zhang, X. Wu, L. i Tan, C. Zou, Y. Liu, Z. Quan, *Small* **2020**, *16*, 1905226.
- [15] Y. Lu, S. Fang, G. Li, L. Li, *J. Alloys Compd.* **2022**, *903*, 163924.
- [16] S. Sadeghi, F. Bateni, T. Kim, D. Y. Son, J. A. Bennett, N. Orouji, V. S. Punati, C. Stark, T. D. Cerra, R. Awad, F. Delgado-Licona, J. Xu, N. Mukhin, H. Dickerson, K. G. Reyes, M. Abolhasani, *Nanoscale* **2024**, *16*, 580.
- [17] A. L. Martins Freitas, A. Tofanello, F. P. Sabino, M. R. Felez, E. A. Morais, S. Brochsztain, J. J. S. Acuña, G. M. Dalpian, J. A. Souza, *ACS Appl. Nano Mater.* **2023**, *6*, 7196.
- [18] J. Sui, J. Yan, D. Liu, K. Wang, G. Luo, *Small* **2020**, *16*, 1902828.
- [19] Z. Jiang, H. Liu, J. Zou, Y. Huang, Z. Xu, D. Pustovyi, S. Vitusevich, *RSC Adv.* **2023**, *13*, 5993.
- [20] L. Lian, M. Zheng, W. Zhang, L. Yin, X. Du, P. Zhang, X. Zhang, J. Gao, D. Zhang, L. Gao, G. Niu, H. Song, R. Chen, X. Lan, J. Tang, J. Zhang, *Adv. Sci.* **2020**, *7*, 2000195.
- [21] Q. A. Akkerman, L. Martínez-Sarti, L. Goldoni, M. Imran, D. Baranov, H. J. Bolink, F. Palazon, L. Manna, *Chem. Mater.* **2018**, *30*, 6915.
- [22] S. Hull, P. Berastegui, *J. Solid State Chem.* **2004**, *177*, 3156.
- [23] R. W. Wyckoff, E. Posnjak, *J. Am. Chem. Soc.* **1922**, *44*, 30.
- [24] Z. Morlin, *Acta Cryst.* **1971**, *27*, 2493.
- [25] Y. Gao, B. Pinho, L. Torrente-Murciano, *Curr. Opin. Chem. Eng.* **2020**, *29*, 26.
- [26] O. Dlugosz, M. Banach, *Chem. Eng.* **2020**, *5*, 1619.
- [27] R. M. Maceiczuk, K. Dümbgen, I. Lignos, L. Protesescu, M. V. Kovalenko, A. J. deMello, *Chem. Mater.* **2017**, *29*, 8433.